MOX-Report No. 27/2018

Numerical solution of fluid-structure interaction problems by means of a high order Discontinuous Galerkin method on polygonal grids

Antonietti, P.F.; Verani, M.; Vergara, C.; Zonca, S.

MOX, Dipartimento di Matematica
Politecnico di Milano, Via Bonardi 9 - 20133 Milano (Italy)

mox-dmat@polimi.it http://mox.polimi.it

Numerical solution of fluid-structure interaction problems by means of a high order Discontinuous Galerkin method on polygonal grids

P.F. Antonietti[♯], M. Verani[♯], C. Vergara[♯], S. Zonca[♯]

April 15, 2018

[♯] MOX– Modellistica e Calcolo Scientifico
Dipartimento di Matematica
Politecnico di Milano
via Bonardi 9, 20133 Milano, Italy
<paola.antonietti,marco.verani,christian.vergara,stefano.zonca>@mate.polimi.it

Keywords: Fluid structure interaction, Discontinuous Galerkin, polygonal meshes

AMS Subject Classification: 65M60 , 74F10 , 65M85

Abstract

We consider the two-dimensional numerical approximation of the fluid-structure interaction problem over unfitted fluid and structure meshes. In particular, we consider a method where the fluid mesh is on the background and fixed, apart at the interface with the moving immersed structure, that cuts the fluid mesh elements generating polygons of arbitrary shape. The new idea of this work is to handle the discretization on such polygons by using the *Discontinuous Galerkin method on polyhedral grids* (PolyDG), which has been recently developed for different differential equations and here adapted for the first time to an heterogeneous problem. We prove a stability result of the proposed semi-discrete formulation and discuss how to deal with the partial or total covering of a fluid mesh element due to the structure movement. We finally present some numerical results with the aim of showing the effectiveness of the proposed method.

1 Introduction

The numerical solution of the problem arising when an immersed structure interacts with a surrounding fluid is very challenging. This fluid-structure interaction (FSI) problem occurs in many applications, for example in the heart where cardiac valves interact with blood [50, 73, 83, 86] and in civil engineering where the wind affects the stability of bridges [33,88], towers [67], and suspended cables [28, 82].

When the structure displacements are large, as happens for the applications mentioned above, the classical *Arbitrary Lagrangian-Eulerian* (ALE) method [54] becomes unfeasible since it would require at each time step a remeshing of the computational domain in order to avoid too stretched elements [71]. For such a reason, other numerical techniques have been developed in order to avoid remeshing techniques. We refer here to strategies based on a fixed background mesh for the fluid and on a moving foreground mesh for the structure. Among them, we mention the *Immersed Boundary* method [31, 32, 62, 65, 75, 79, 80] and the *Fictitious Domain* (FD) method [61,65], for example. Another, more recent, strategy is the *Cut-Finite Element* method (Cut-FEM), where the weak formulations of the two sub-problems are written at each time step in the physical computational domains and then glued together by means of suitable mortaring techniques, usually the Discontinuous Galerkin (DG) method, see, e.g., [38, 74]. Since the fluid problem is solved in an Eulerian framework, the fluid-structure (FS) interface moves, whereas the fluid background mesh is fixed; therefore, such an approach requires to handle general (possibly polygonal) elements close to the FS interface, which are generated by the intersection of the structure boundaries with the background mesh elements.

In order to deal with general-shaped mesh elements, the *eXtended Finite Elements* method (XFEM) has been proposed in [66] for the Poisson problem, then extended to the FSI problem in [1] for the case of a membrane structure and in [89] for general thick structures and three-dimensional simulations. The idea of XFEM is to consider, on the background cut elements, the basis functions of the original triangle (tetrahedron) and build the solution over the whole original element, then ignoring it in the portion of the triangle (tetrahedron) covered by the structure. In particular, in two dimensions, whenever a triangle is cut into three parts by a thin structure (two uncovered parts within a covered one in the middle), the XFEM recovers a numerical solution by doubling the degrees of freedom (dofs) of the original triangle. XFEM is an effective strategy, that allows to recover optimal convergence for linear approximations of the Poisson problem [66] and accurate results for FSI [1, 89]. Nevertheless, the extension and implementation of this formulation for high-order approximations, three-dimensional configurations, and possibly degenerate mesh elements (very small angles/interesections) is a hard task. Indeed, at the best of our knowledge, only first order XFEM have been proposed so far for FSI problems. Moreover, stability of the formulation is guaranteed only under quite strong regularity geometric assumptions on the mesh element or by adding a suitable "ghost" stabilization term [37].

In this paper, we introduce and analyze a new way to handle polygonal fluid elements generated by the intersection with the moving structure. The idea is to consider a numerical method to handle directly the polygonal elements. Several numerical discretization methods which admit polygonal/polyhedral meshes have been proposed within the current literature; here, we mention, for example, the *Composite Finite Elements* method [5,63,64], the *Mimetic Finite Difference* (MFD) method [4,27,34–36,70], the *Polygonal Finite Elements* method [84], the *Virtual Element Method* (VEM) [3,9,18,24–26,29,30,46], the *Hybrid High-Order* (HHO) method [51–53], and the *Gradient Schemes* [55]. Here, we consider the recently developed *Discontinuous Galerkin method on polyhedral grids* (PolyDG), see, e.g., [2,6–8,11,13–15,21–23,41–44,49,60,72,76,87]. In PolyDG the DG Finite Elements spaces are defined directly over polygonal elements resulting from the interesection of the meshes. With this strategy, high order accuracy can be achieved in any space dimension by introducing suitable modal basis functions directly in the physical frame configuration. The proposed formulation allows for very general polygonal meshes with possibly degenerate edges and without any assumption on the number of edges that each polygon can have, thus being perfectly suited for mesh agglomeration and intersections. Finally, as PolyDG methods can be seen as the evolution of the classical DG approach, they are naturally oriented towards 3D scalable implementations. To the best of our knowledge, this is the first attempt to exploit the flexibility offered by polygonal grids to efficiently handle problems posed on moving domains or interfaces.

The summary of the paper is as follows. In Sect. 2 we introduce the strong formulation of the FSI problem, in Sect. 3 we introduce the corresponding PolyDG approximation. In Sect. 4 we provide a stability result for the semi-discretized problem, and in Sect. 5 we show several two-dimensional numerical results aiming at demonstrating the effectiveness of the proposed strategy.

2 Continuous formulations of the fluid-structure interaction problem

In this section, we introduce the continuous problems we are interested in. In particular, referring to Figure 1, we consider a fluid domain $\Omega_f(t)$ and a structure domain $\Omega_s(t)$, both changing in time, such that $\Omega = \Omega_f(t) \cup \Omega_s(t) \subset \mathbb{R}^2$, being $\Sigma(t)$ the fluid-structure interface. We set $\Gamma_f = \partial\Omega_f(t) \setminus \Sigma(t)$, $\Gamma_f \neq \emptyset$, and $\Gamma_s = \partial\Omega_s(t) \setminus \Sigma(t)$, $\Gamma_s \neq \emptyset$ (for simplicity, both supposed not changing in time). Finally, we denote by $\boldsymbol{n}(t)$ the outward unit normal vector to the fluid domain.

Since the structure problem is solved in a Lagrangian framework, we need to introduce the reference configuration of the solid domain, which will be denoted by the superscript $\widehat{\ }$. For any $t > 0$, the material domain $\Omega_s(t)$ is the image of $\widehat{\Omega}_s$ by a Lagrangian map $\mathcal{L}(t) : \widehat{\Omega}_s \to \Omega_s(t)$. We use the notation $\widehat{g} = g \circ \mathcal{L}(t)$ to denote in $\widehat{\Omega}_s$ any function g defined in the current solid configuration $\Omega_s(t)$. On the contrary, as usual, the fluid problem is written in an Eulerian framework.

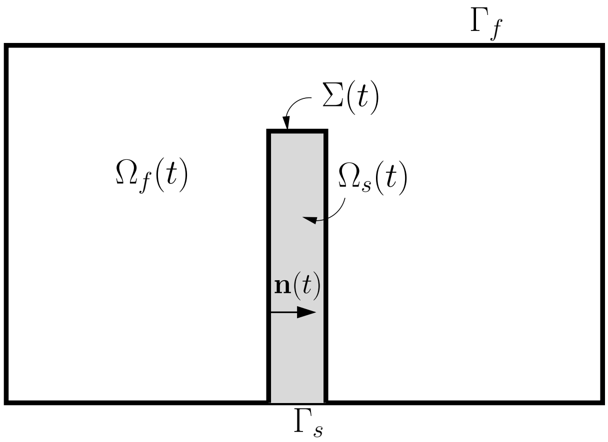

Figure 1: Fluid and structure domains $\Omega_f(t)$ and $\Omega_s(t)$, respectively, and fluid-structure interface $\Sigma(t)$. Notice that $\Omega_s(t)$ could be completely immersed in the fluid domain.

2.1 Strong formulation

Given a final observation time $T > 0$, the strong formulation of the fluid-structure interaction problem reads as follows: for each $t \in (0, T]$, find the fluid velocity $\boldsymbol{u}$, the fluid pressure p, and the solid displacement $\boldsymbol{d}$, such that

$$\rho_f \partial_t \boldsymbol{u} - \nabla \cdot \boldsymbol{T}_f(\boldsymbol{u}, p) = \boldsymbol{f}_f \qquad \text{in } \Omega_f(t), \tag{1a}$$
$$\nabla \cdot \boldsymbol{u} = \boldsymbol{0} \qquad \text{in } \Omega_f(t), \tag{1b}$$
$$\boldsymbol{u} = \boldsymbol{0} \qquad \text{on } \Gamma_f, \tag{1c}$$
$$\rho_s \partial_{tt} \widehat{\boldsymbol{d}} - \nabla \cdot \widehat{\boldsymbol{T}}_s(\widehat{\boldsymbol{d}}) = \widehat{\boldsymbol{f}}_s \qquad \text{in } \widehat{\Omega}_s, \tag{1d}$$
$$\widehat{\boldsymbol{d}} = \boldsymbol{0} \qquad \text{on } \widehat{\Gamma}_s, \tag{1e}$$
$$\boldsymbol{u} = \partial_t \boldsymbol{d} \qquad \text{on } \Sigma(t), \tag{1f}$$
$$\boldsymbol{T}_f(\boldsymbol{u}, p)\boldsymbol{n} = \boldsymbol{T}_s(\boldsymbol{d})\boldsymbol{n} \qquad \text{on } \Sigma(t), \tag{1g}$$

where (1a)-(1c) are the Stokes equations, (1d)-(1e) are the equations of the elastodynamics, and (1f)-(1g) are the physical coupling conditions, written in the current configuration. Moreover, ρ_f and ρ_s are the fluid and structure densities, respectively, $\boldsymbol{f}_f$ and $\boldsymbol{f}_s$ are two forcing terms, $\boldsymbol{T}_f(\boldsymbol{u}, p) = -p\boldsymbol{I} + 2\mu_f \boldsymbol{D}(\boldsymbol{u})$ is the fluid Cauchy stress tensor, $\boldsymbol{T}_s(\boldsymbol{d}) = \lambda_s(\nabla \cdot \boldsymbol{d})\boldsymbol{I} + 2\mu_s \boldsymbol{D}(\boldsymbol{d})$ is the solid stress tensor, with $\boldsymbol{D}(\boldsymbol{w}) = \dfrac{1}{2}(\nabla \boldsymbol{w} + \nabla \boldsymbol{w}^T)$, μ_f is the fluid dynamic viscosity, $\lambda_s, \mu_s > 0$ are the Lamé parameters. We have used the following identity to pass from the Piola-Kirchhoff tensor $\widehat{\boldsymbol{T}}_s(\widehat{\boldsymbol{d}})$ to the Cauchy stress tensor $\boldsymbol{T}_s(\boldsymbol{d})$:

$$\widehat{\boldsymbol{T}}_s = J \boldsymbol{T}_s \boldsymbol{F}^{-T}.$$

Here, $J = \det(\boldsymbol{F})$, $\boldsymbol{F} = \nabla \boldsymbol{x}$ is the deformation tensor, where the gradient is taken with respect to the reference space coordinates, and $\boldsymbol{x}$ are the points coordinates in the current configuration.

Problem (1) is supplemented with the initial conditions $\boldsymbol{u}(\boldsymbol{x},0) = \boldsymbol{u}^0(\boldsymbol{x})$, $\boldsymbol{d}(\boldsymbol{x},0) = \boldsymbol{d}^0(\boldsymbol{x})$ and $\partial_t \boldsymbol{d}(\boldsymbol{x},0) = \boldsymbol{v}^0(\boldsymbol{x})$.

Remark 1. *Notice that, in this work, we consider the Stokes and the Hooke linear problems. This simple choice allows us to focus on the novel contribution of the paper, without adding further technical difficulties due to the presence of non-linearities. The generalization to the more realistic Navier-Stokes/Finite Elasticity coupled problem is under investigation.*

Remark 2. *Notice that in* (1c), *we have set for the sake of simplicity homogeneous Dirichlet conditions for the fluid on the boundary different from the fluid-structure interface. Of course, in real scenarios, non-homogeneous and/or Neumann conditions should be considered for the fluid on Γ_f. This is the case of the numerical results reported in Sect. 4.*

2.2 Weak formulation

We consider a *penalty weak formulation* for the Stokes problem (1a)-(1c). In particular, the incompressibility constraint (1b) is enforced by penalization rather than by means of a Lagrange multiplier (the pressure). Thus, the pressure p disappears in the weak formulation.

We preliminary introduce the spaces

$$\boldsymbol{V}_f(t) = \left\{ \boldsymbol{v} \in \left[H^1(\Omega_f(t))\right]^2, \boldsymbol{v}_{|\Gamma_f} = \boldsymbol{0} \right\}$$
$$\boldsymbol{V}_s = \left\{ \widehat{\boldsymbol{w}} \in \left[H^1(\widehat{\Omega}_s)\right]^2, \widehat{\boldsymbol{w}}_{|\widehat{\Gamma}_s} = \boldsymbol{0} \right\}.$$

Then, the weak formulation of problem (1) reads as follows: for $t \in (0,T]$, find $(\boldsymbol{u}(t), \widehat{\boldsymbol{d}}(t)) \in \boldsymbol{V}_f(t) \times \boldsymbol{V}_s$ such that $\boldsymbol{u}|_\Sigma = \partial_t \boldsymbol{d}|_\Sigma$, and

$$\rho_f(\partial_t \boldsymbol{u}, \boldsymbol{v})_{\Omega_f} + a_f(\boldsymbol{u}, \boldsymbol{v}) + \rho_s(\partial_{tt}\widehat{\boldsymbol{d}}, \widehat{\boldsymbol{w}})_{\widehat{\Omega}_s} + a_s(\widehat{\boldsymbol{d}}, \widehat{\boldsymbol{w}}) = (\boldsymbol{f}_f, \boldsymbol{v})_{\Omega_f} + (\widehat{\boldsymbol{f}}_s, \widehat{\boldsymbol{w}})_{\widehat{\Omega}_s}, \quad (2)$$

for all $(\boldsymbol{v}(t), \widehat{\boldsymbol{w}}) \in \boldsymbol{V}_f(t) \times \boldsymbol{V}_s$ such that $\boldsymbol{v}_{|\Sigma} = \boldsymbol{w}_{|\Sigma}$. We have denoted by $(\cdot,\cdot)_Z$ the L^2-inner products over the domain Z. In (2), the bilinear forms $a_f : \boldsymbol{V}_f(t) \times \boldsymbol{V}_f(t) \to \mathbb{R}$ and $a_s : \boldsymbol{V}_s \times \boldsymbol{V}_s \to \mathbb{R}$ are defined as

$$a_f(\boldsymbol{u}, \boldsymbol{v}) = \left(\widetilde{\boldsymbol{T}}_f(\boldsymbol{u}), \nabla \boldsymbol{v}\right)_{\Omega_f} = \lambda_f \left(\nabla\cdot\boldsymbol{u}, \nabla\cdot\boldsymbol{v}\right)_{\Omega_f} + 2\mu_f \left(\boldsymbol{D}(\boldsymbol{u}), \boldsymbol{D}(\boldsymbol{v})\right)_{\Omega_f},$$

$$a_s\left(\widehat{\boldsymbol{d}}, \widehat{\boldsymbol{w}}\right) = \left(\widehat{\boldsymbol{T}}_s(\widehat{\boldsymbol{d}}), \nabla\widehat{\boldsymbol{w}}\right)_{\widehat{\Omega}_s} = \lambda_s \left(\nabla\cdot\widehat{\boldsymbol{d}}, \nabla\cdot\widehat{\boldsymbol{w}}\right)_{\widehat{\Omega}_s} + 2\mu_s \left(\boldsymbol{D}(\widehat{\boldsymbol{d}}), \boldsymbol{D}(\widehat{\boldsymbol{w}})\right)_{\widehat{\Omega}_s}, \quad (3)$$

respectively, where $\widetilde{\boldsymbol{T}}_f(\boldsymbol{u}) = \lambda_f(\nabla\cdot\boldsymbol{u})\boldsymbol{I} + 2\mu_f\boldsymbol{D}(\boldsymbol{u})$. The new parameter λ_f plays the role of the penalty parameter for the incompressibility constraint.

Remark 3. *Notice that in* (2) *we have considered a penalty formulation instead of the classical saddle-point one [85]. This choice has been motivated by implementation issues, since in such a way the Stokes and Hooke problems are formulated by means of similar bilinear forms. It has been proven in [85] that the continuous penalized velocity solution converges to the one obtained by means of the saddle point formulation. Moreover, the pressure can be estimated a posteriori [47], see also [69]. It is worth to remark that the specific features of the proposed formulation can be easily extended to the case where the incompressibility constraint is enforced by means of a Lagrange multiplier.*

Notice that, owing to the following relation (used to estimate the pressure a posteriori)

$$p = \lim_{\lambda_f \to \infty} \lambda_f \nabla \cdot \boldsymbol{u},$$

cf. [47], we have

$$\widetilde{\boldsymbol{T}}_f(\boldsymbol{u}) = \boldsymbol{T}_f(\boldsymbol{u}, p) \quad \text{for } \lambda_f \to \infty, \tag{4}$$

where, with an abuse of notation, we have denoted by $\boldsymbol{u}$ both the solutions of the penalty and Lagrange multiplier formulations. Thus, (4) ensures that the dynamic interface condition (1g) is enforced also in (2) in the limit $\lambda_f \to \infty$.

3 Discontinuous Galerkin method on polygonal grids

In this section, we introduce the discretization of problem (2) by means of *P*olyDG methods for the space discretization coupled with a *Backward Difference Formula* for the time integration.

3.1 Space discretization

To ease the presentation, we assume that $\Omega_f(t)$, $\Omega_s(t)$ and $\Sigma(t)$ are polygonal domains with Lipschitz boundaries. We denote by $\mathcal{T}_{s,h}(t)$ a solid mesh covering the domain $\Omega_s(t)$ and fitted to $\partial\Omega_s(t)$ and by $\widehat{\mathcal{T}}_{s,h}$ the mesh corrisponding to the reference configuration $\widehat{\Omega}_s$. Accordingly, we denote by $\mathcal{T}_h$ the background mesh, covering the whole domain $\Omega = \Omega_f(t) \cup \Omega_s(t)$ and fitted to Γ_f, but in general not to $\Sigma(t)$ and Γ_s. Notice that $\mathcal{T}_{s,h}(t)$ changes with time, whereas $\mathcal{T}_h$ is fixed. We indicate with $h > 0$ the space discretization parameter which is a function that may vary among the elements K of the meshes and between the background and structure meshes. As result, the solid mesh $\mathcal{T}_{s,h}(t)$ overlaps the background mesh $\mathcal{T}_h$, see Figure 2, left. Note that both $\mathcal{T}_h$ and $\mathcal{T}_{s,h}(t)$ can be made of arbitrarily shaped, possibly non-convex, polygons. Moreover, we define the mesh $\widetilde{\mathcal{T}}_h(t)$ composed of the elements of the background mesh $\mathcal{T}_h$ that are intersected by foreground structure mesh $\mathcal{T}_{s,h}(t)$, i.e.

$$\widetilde{\mathcal{T}}_h(t) = \{K : K \in \mathcal{T}_h(t), K \cap \mathcal{T}_{s,h}(t) \neq \emptyset\}.$$

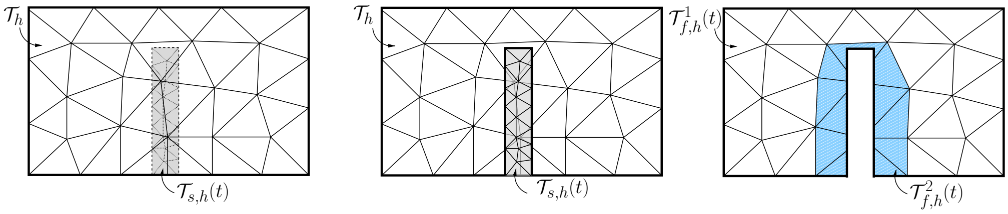

Figure 2: Left: Background mesh $\mathcal{T}_h$; Middle: The structure mesh $\mathcal{T}_{s,h}(t)$ overlaps the background mesh $\mathcal{T}_h$. Right: Fluid mesh $\mathcal{T}_{f,h}(t)$ obtained by cutting the elements of the background mesh $\mathcal{T}_h$. Notice the polygons generated in the fluid mesh $\mathcal{T}^2_{f,h}(t)$.

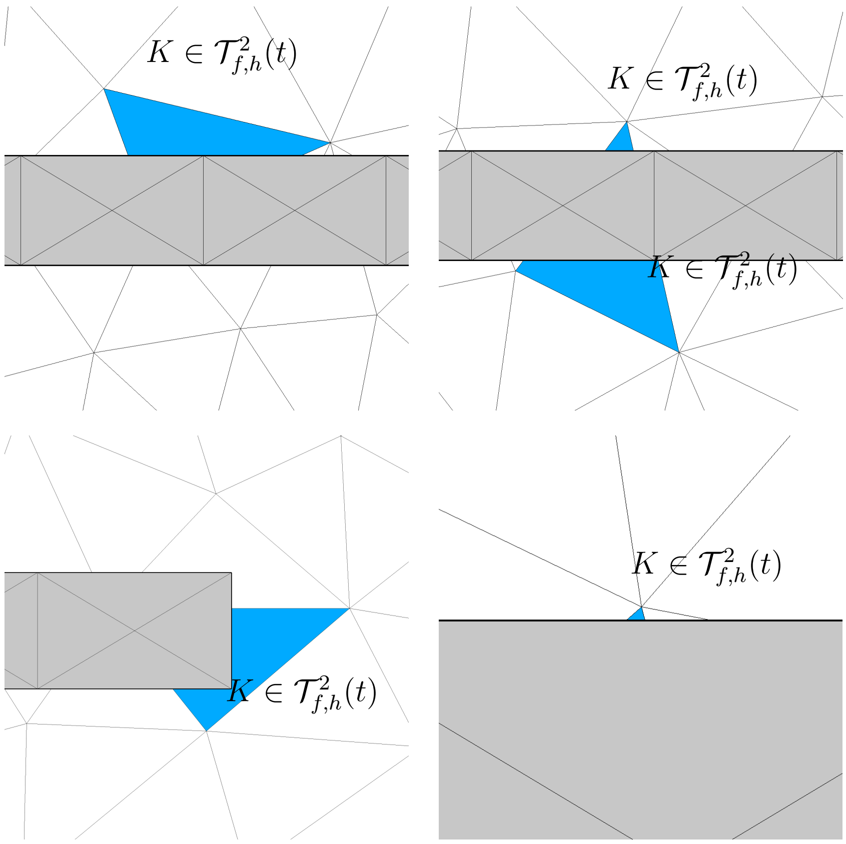

Figure 3: Possible geometric intersections between the background mesh $\mathcal{T}_h$ and the solid mesh $\mathcal{T}_{s,h}(t)$ (in grey): examples of the resulting chopped elements $K \in \mathcal{T}^2_{f,h}(t)$ are depicted in blue.

We introduce now the fluid mesh $\mathcal{T}_{f,h}(t)$ obtained by chopping the elements of the background mesh $\mathcal{T}_h$ as a result of the intersection with the foreground structure mesh $\mathcal{T}_{s,h}(t)$. More precisely, we set $\mathcal{T}_{f,h}(t) = \mathcal{T}^1_{f,h}(t) \cup \mathcal{T}^2_{f,h}(t)$, where

$$\begin{aligned}
&\mathcal{T}^1_{f,h}(t) = \{K \in \mathcal{T}_h : K \cap K_s = \emptyset, \ \forall K_s \in \mathcal{T}_{s,h}(t)\},\\
&\mathcal{T}^2_{f,h}(t) = \{K_f \subset \Omega_f(t) : K_f = K \setminus \bigcup_{\substack{K_s \in \mathcal{T}_{s,h}(t)\\ K_s \cap K \neq \emptyset}} K_s, \ \text{for } K \in \widetilde{\mathcal{T}}_h(t)\},
\end{aligned}$$

see Figure 2, right, and Figure 3. Notice that the fluid elements belonging to $\mathcal{T}^2_{f,h}(t)$ are in general polygons even in the case of original triangular background and solid meshes (see Figure 2, right, and Figure 3) and they can be non-convex and with possibly degenerate edges.

Remark 4. *According to [45], see also [8], very general decompositions can be allowed in the framework of Discontinuous Galerkin discretizations, like the one we will address. For example no limitations are imposed on either the relative size of a face of an element compared to its diameter, nor on the total number of faces an element could have.*

We introduce now the Discontinuous Galerkin approximation of problem (2) on polygonal meshes (PolyDG). Given a positive integer l, to each $\mathcal{T}_{i,h}$, $i = \{f, s\}$, we associate the corresponding DG Finite Elements space defined as

$$\begin{aligned}
&\boldsymbol{V}^l_{f,h}(t) = \{\boldsymbol{v}(t) \in [L^2(\Omega_f(t))]^2 : \boldsymbol{v}|_K \in [\mathcal{P}_l(K)]^2, \forall K \in \mathcal{T}_{f,h}(t)\},\\
&\boldsymbol{V}^l_{s,h} = \{\boldsymbol{v} \in [L^2(\widehat{\Omega}_s)]^2 : \boldsymbol{v}|_K \in [\mathcal{P}_l(K)]^2, \forall K \in \widehat{\mathcal{T}}_{s,h}\},
\end{aligned} \tag{5}$$

where $\mathcal{P}_l(K)$ denotes the space of polynomials on K of total degree at most l. We remark that the fluid discrete space and its elements are functions of time since Ω_f changes in time, whereas the structure discrete space and its elements do not change in time since they refer to the reference configuration $\widehat{\Omega}_s$.

Remark 5. *Notice that in the previous definitions of the discrete spaces $\boldsymbol{V}^l_{f,h}(t)$ and $\boldsymbol{V}^l_{s,h}$ we have assumed, for the sake of notation, that l is constant over all mesh elements. Element-wise varying polynomial approximation degrees can be considered as well, under suitable local-bounded variation assumptions.*

An interior face F_i (notice that since we are addressing the case $d = 2$, "face" means "edge") of $\mathcal{T}_{i,h}(t)$, $i = \{f, s\}$, is defined as the (non–empty) interior of $\partial \overline{K_i}^+ \cap \partial \overline{K_i}^-$, where $K_i^{\pm}$ are two adjacent elements of $\mathcal{T}_{i,h}(t)$, $i = \{f, s\}$. Similarly, a boundary face of $\mathcal{T}_{i,h}(t)$, $i = \{f, s\}$, is defined as the (non-empty) interior of $\partial \overline{K_i} \cap \Gamma_i(t)$, where K_i is an element of $\mathcal{T}_{i,h}(t)$, $i = \{f, s\}$. We collect the interior and boundary faces F_i in the sets $\mathcal{F}_{i,h}(t)$, $i = \{f, s\}$. Notice that, by construction, any face $F_i \in \mathcal{F}_{i,h}(t)$, $i = \{f, s\}$, is not contained in Σ. The faces F_Σ belonging to $\Sigma(t)$ are collected in the set $\mathcal{F}_{\Sigma,h}(t)$.

Next, following the notation introduced in [16], we introduce suitable trace operators, cf also [17]. Let F be an interior face belong to one of $\mathcal{F}_{i,h}(t)$, $i=\{f,s,\Sigma\}$, shared by two elements $K^{\pm}$, and let $\boldsymbol{n}^{\pm}$ denote the normal unit vectors on F pointing outward $K^{\pm}$, respectively. For (regular enough) vector-valued and symmetric tensor-valued functions $\boldsymbol{v}$ and $\boldsymbol{T}$, respectively, we define the *weighted average* and *jump* operators as

$$\{\boldsymbol{T}\}=\frac{1}{2}\left(\boldsymbol{T}^{+}\boldsymbol{n}^{+}+\boldsymbol{T}^{-}\boldsymbol{n}^{-}\right), \qquad [\![\boldsymbol{v}]\!]=\boldsymbol{v}^{+}\odot\boldsymbol{n}^{+}+\boldsymbol{v}^{-}\odot\boldsymbol{n}^{-},$$

where $\boldsymbol{v}^{\pm}$ and $\boldsymbol{T}^{\pm}$ denote the traces of $\boldsymbol{v}$ and $\boldsymbol{T}$ on F taken within the interior of $K^{\pm}$, respectively, and where $\boldsymbol{v}\odot\boldsymbol{n}=(\boldsymbol{v}\boldsymbol{n}^{T}+\boldsymbol{n}\boldsymbol{v}^{T})/2$. Notice that $[\![\boldsymbol{v}]\!]$ is a symmetric tensor-valued function. On a boundary face F, due to the homogeneous Dirichlet conditions, we set analogously

$$\{\boldsymbol{T}\}=\boldsymbol{T}\boldsymbol{n}, \qquad [\![\boldsymbol{v}]\!]=\boldsymbol{v}\odot\boldsymbol{n}.$$

The semi-discrete PolyDG approximation to (2) reads as follows: Given $\delta\in[0,1]$, $\boldsymbol{f}_f\in[L^2(\Omega_f)]^d$, and $\boldsymbol{f}_s\in[L^2(\Omega_s)]^d$, for any $t\in(0,T]$, find $(\boldsymbol{u}_h(t),\widehat{\boldsymbol{d}}_h(t))\in\boldsymbol{V}^l_{f,h}(t)\times\boldsymbol{V}^l_{s,h}$ such that

$$A_{f,h}\left(\boldsymbol{u}_h,\boldsymbol{v}_h\right)+A_{s,h}\left(\widehat{\boldsymbol{d}}_h,\widehat{\boldsymbol{w}}_h\right)+A_{\Sigma,h}(\boldsymbol{u}_h,\boldsymbol{d}_h;\boldsymbol{v}_h,\boldsymbol{w}_h)=F(\boldsymbol{v}_h,\widehat{\boldsymbol{w}}_h), \tag{6}$$

for all $(\boldsymbol{v}_h,\widehat{\boldsymbol{w}}_h)\in\boldsymbol{V}^l_{f,h}(t)\times\boldsymbol{V}^l_{s,h}$. Here, we have set

$$\begin{aligned}
A_{f,h}\left(\boldsymbol{u}_h,\boldsymbol{v}_h\right)&=\rho_f\left(\partial_t\boldsymbol{u}_h,\boldsymbol{v}_h\right)_{\Omega_f}+a_f\left(\boldsymbol{u}_h,\boldsymbol{v}_h\right)-\left(\left\{\widetilde{\boldsymbol{T}}_f(\boldsymbol{u}_h)\right\},[\![\boldsymbol{v}_h]\!]\right)_{\mathcal{F}_{f,h}}-\left([\![\boldsymbol{u}_h]\!],\left\{\widetilde{\boldsymbol{T}}_f(\boldsymbol{v}_h)\right\}\right)_{\mathcal{F}_{f,h}}\\
&\quad+\left(\sigma_f[\![\boldsymbol{u}_h]\!],[\![\boldsymbol{v}_h]\!]\right)_{\mathcal{F}_{f,h}}, \qquad\qquad (7a)\\
A_{s,h}\left(\widehat{\boldsymbol{d}}_h,\widehat{\boldsymbol{w}}_h\right)&=\rho_s\left(\partial_{tt}\widehat{\boldsymbol{d}}_h,\widehat{\boldsymbol{w}}_h\right)_{\widehat{\Omega}_s}+a_s\left(\widehat{\boldsymbol{d}}_h,\widehat{\boldsymbol{w}}_h\right)-\left(\left\{\widehat{\boldsymbol{T}}_s(\widehat{\boldsymbol{d}}_h)\right\},[\![\widehat{\boldsymbol{w}}_h]\!]\right)_{\widehat{\mathcal{F}}_{s,h}}-\left([\![\widehat{\boldsymbol{d}}_h]\!],\left\{\widehat{\boldsymbol{T}}_s(\widehat{\boldsymbol{w}}_h)\right\}\right)_{\widehat{\mathcal{F}}_{s,h}}\\
&\quad+\left(\widehat{\sigma}_s[\![\widehat{\boldsymbol{d}}_h]\!],[\![\widehat{\boldsymbol{w}}_h]\!]\right)_{\widehat{\mathcal{F}}_{s,h}}, \qquad\qquad (7b)\\
A_{\Sigma,h}(\boldsymbol{u}_h,\boldsymbol{d}_h;\boldsymbol{v}_h,\boldsymbol{w}_h)&=-\left(\delta\widetilde{\boldsymbol{T}}_f(\boldsymbol{u}_h)\boldsymbol{n}+(1-\delta)\boldsymbol{T}_s(\boldsymbol{d}_h)\boldsymbol{n},\boldsymbol{v}_h-\boldsymbol{w}_h\right)_{\mathcal{F}_{\Sigma,h}}\\
&\quad-\left(\boldsymbol{u}_h-\partial_t\boldsymbol{d}_h,\delta\widetilde{\boldsymbol{T}}_f(\boldsymbol{v}_h)\boldsymbol{n}+(1-\delta)\boldsymbol{T}_s(\boldsymbol{w}_h)\boldsymbol{n}\right)_{\mathcal{F}_{\Sigma,h}}+\left(\sigma_\Sigma(\boldsymbol{u}_h-\partial_t\boldsymbol{d}_h),\boldsymbol{v}_h-\boldsymbol{w}_h\right)_{\mathcal{F}_{\Sigma,h}},\\
&\qquad\qquad (7c)\\
F(\boldsymbol{v}_h,\widehat{\boldsymbol{w}}_h)&=\left(\boldsymbol{f}_f,\boldsymbol{v}_h\right)_{\Omega_f}+\left(\boldsymbol{f}_s,\widehat{\boldsymbol{w}}_h\right)_{\widehat{\Omega}_s},
\end{aligned}$$

with $a_f(\cdot,\cdot)$ and $a_s(\cdot,\cdot)$ defined in (3). In (6), we have denoted by $\sigma_\Sigma\in L^\infty(\mathcal{F}_{\sigma,h})$, $\sigma_f\in L^\infty(\mathcal{F}_{f,h})$ and $\widehat{\sigma}_s\in L^\infty(\widehat{\mathcal{F}}_{s,h})$ the three positive penalty functions related to the face belonging to $\mathcal{F}_{i,h}$, $i = \{\Sigma, f, s\}$, respectively. Their definition is given by

$$\begin{aligned}
\sigma_f &= \gamma_f \max_{K^+,K^-} \left\{ \frac{l^2 \bar{\mathcal{C}}_{f,K}}{h_K} \right\}, & \overline{F} = \partial\overline{K^+} \bigcap \partial\overline{K^-} \in \mathcal{F}_{f,h}, \\
\widehat{\sigma}_s &= \gamma_s \max_{K^+,K^-} \left\{ \frac{l^2 \bar{\mathcal{C}}_{s,K}}{h_K} \right\}, & \overline{F} = \partial\overline{K^+} \bigcap \partial\overline{K^-} \in \widehat{\mathcal{F}}_{s,h}, \\
\sigma_\Sigma &= \gamma_\Sigma \max_{K^+,K^-} \left\{ \frac{l^2}{h_K} \left(\delta \bar{\mathcal{C}}_{f,K} + (1-\delta) \bar{\mathcal{C}}_{s,K} \right) \right\}, & \overline{F} = \partial\overline{K^+} \bigcap \partial\overline{K^-} \in \mathcal{F}_{\Sigma,h},
\end{aligned} \tag{8}$$

h_K being the mesh size of the element K, $\bar{\mathcal{C}}_{f,K} = \|\mathcal{C}_f|_K\|_{l^2}$, $\bar{\mathcal{C}}_{s,K} = \|\mathcal{C}_s|_K\|_{l^2}$, with $\mathcal{C}_f$ and $\mathcal{C}_s$ the fourth order elastic tensors such that $\widetilde{\boldsymbol{T}}_f(\boldsymbol{u}) = \mathcal{C}_f \boldsymbol{D}(\boldsymbol{u})$ and $\boldsymbol{T}_s(\boldsymbol{d}) = \mathcal{C}_s \boldsymbol{D}(\boldsymbol{d})$, which are supposed to be piecewise constant over the mesh. Moreover, γ_Σ, γ_f and γ_s are positive constants that will be chosen later on. In the form $A_{\Sigma,h}(\cdot,\cdot;\cdot,\cdot)$ in (6) we have the DG terms (consistency, symmetry, and stability terms) related to the FS interface $\Sigma(t)$ which guarantee the weak imposition of the physical interface conditions (1f)-(1g), whereas in the forms $A_{f,h}(\cdot,\cdot)$ and $A_{s,h}(\cdot,\cdot)$ we have the DG terms in the fluid and structure domains separately. Notice also that at the fluid-structure interface Σ we have used a weighted average DG formulation with parameter $\delta \in [0,1]$, see (6c).

We notice that the idea of using a DG mortaring to weakly impose the continuity conditions at the fluid-structure interface was first introduced, for the case of fitted meshes, in [39, 40].

3.2 Stability of the semi-discrete problem

In this section, we prove a stability result of the semi-discrete formulation (5). To this aim, we define the following norms:

$$\begin{aligned}
\|\widehat{\boldsymbol{w}}_h\|^2_{s,h} &= \left\| \rho_s^{1/2} \partial_t \widehat{\boldsymbol{w}}_h \right\|^2_{\widehat{\Omega}_s} + \|\widehat{\boldsymbol{w}}_h\|^2_{DG,s}, \\
\|(\boldsymbol{v}_h, \boldsymbol{w}_h)\|^2_{\Sigma,h} &= \left\| \sigma_\Sigma^{1/2} \left(\boldsymbol{v}_h - \partial_t \boldsymbol{w}_h \right) \right\|^2_{\mathcal{F}_{\Sigma,h}}, \\
\|\boldsymbol{v}_h\|^2_{DG,f} &= a_f\left(\boldsymbol{v}_h, \boldsymbol{v}_h\right) + \left\| \sigma_f^{1/2} [\![\boldsymbol{v}_h]\!] \right\|^2_{\mathcal{F}_{f,h}}, \\
\|\widehat{\boldsymbol{w}}_h\|^2_{DG,s} &= a_s\left(\widehat{\boldsymbol{w}}_h, \widehat{\boldsymbol{w}}_h\right) + \left\| \widehat{\sigma}_s^{1/2} [\![\widehat{\boldsymbol{w}}_h]\!] \right\|^2_{\widehat{\mathcal{F}}_{s,h}}.
\end{aligned} \tag{9}$$

We consider in what follows some preliminary results useful to prove the final estimate.

The first result regards an inverse estimate which is valid on polygons, is sharp with respect to facet degeneration, and holds without any limitation on the number of edges that an element can have. To this aim, taking as a reference [41], we make first the following assumption on the mesh.

Assumption 1. *For any mesh element K, there exists a set of non-overlapping triangles T_i, $i = 1, \ldots, n_K$, contained in K, such that for any edge $F \subset \partial K$, it* *holds that $\overline{F} = \partial\overline{K} \cap \partial\overline{T_i}$ for some i, and the diameter h_K of K can be bounded by*

$$h_K \lesssim \frac{|T_i|}{|F|}, \quad \forall\, l = 1, \dots, n_K.$$

The hidden constant is independent of the discretization parameters, the number of edges of the element K, and the edge measures.

Under Assumption 1, the following inverse estimate holds true for a tensorial function S which is a piecewise polynomial over the mesh:

$$\|S\|_{\partial K} \lesssim \frac{l}{h_K^{1/2}} \|S\|_K \,, \tag{10}$$

cf [41].

Lemma 1. *If the penalty parameter γ_f is large enough and Assumption 1 holds true for any element $K \in \mathcal{T}_{f,h}$, then there exists a positive constant α_f such that*

$$A_{f,h}(\boldsymbol{u}_h, \boldsymbol{u}_h) \gtrsim \frac{1}{2}\frac{d}{dt}\left\|\rho_f^{1/2}\boldsymbol{u}_h\right\|_{\Omega_f}^2 + \alpha_f \|\boldsymbol{u}_h\|_{DG,f}^2 \,. \tag{11}$$

Proof. By using the definition of $A_{f,h}(\cdot,\cdot)$, cf (6a), and the Cauchy-Schwarz inequality, we obtain

$$\begin{aligned} A_{f,h}(\boldsymbol{u}_h, \boldsymbol{u}_h) &= \rho_f (\partial_t \boldsymbol{u}_h, \boldsymbol{u}_h)_{\Omega_f} + a_f(\boldsymbol{u}_h, \boldsymbol{u}_h) - 2\left(\left\{\widetilde{\boldsymbol{T}}_f(\boldsymbol{u}_h)\right\}, [\![\boldsymbol{u}_h]\!]\right)_{\mathcal{F}_{f,h}} + (\sigma_f [\![\boldsymbol{u}_h]\!], [\![\boldsymbol{u}_h]\!])_{\mathcal{F}_{f,h}} \\ &= \frac{1}{2}\frac{d}{dt}\left\|\rho_f^{1/2}\boldsymbol{u}_h\right\|_{\Omega_f}^2 + \|\boldsymbol{u}_h\|_{DG,f}^2 - 2\left(\left\{\widetilde{\boldsymbol{T}}_f(\boldsymbol{u}_h)\right\}, [\![\boldsymbol{u}_h]\!]\right)_{\mathcal{F}_{f,h}} \\ &\geq \frac{1}{2}\frac{d}{dt}\left\|\rho_f^{1/2}\boldsymbol{u}_h\right\|_{\Omega_f}^2 + \|\boldsymbol{u}_h\|_{DG,f}^2 - 2\left\|\sigma_f^{-1/2}\left\{\widetilde{\boldsymbol{T}}_f(\boldsymbol{u}_h)\right\}\right\|_{\mathcal{F}_{f,h}} \left\|\sigma_f^{1/2}[\![\boldsymbol{u}_h]\!]\right\|_{\mathcal{F}_{f,h}}. \end{aligned} \tag{12}$$

Next, noticing that the faces belonging to $\mathcal{F}_{f,h}$ are a subset of all the faces in $\mathcal{T}_{f,h}$, and that $\widetilde{\boldsymbol{T}}_f(\boldsymbol{u}_h)$ is a piecewise polynomial over $\mathcal{T}_{f,h}$, we have from (9):

$$\left\|\sigma_f^{-1/2}\left\{\widetilde{\boldsymbol{T}}_f(\boldsymbol{u}_h)\right\}\right\|_{\mathcal{F}_{f,h}} \lesssim \left(\sum_{K\in\mathcal{T}_{f,h}} \left\|\sigma_f^{-1/2}\widetilde{\boldsymbol{T}}_f(\boldsymbol{u}_h)\right\|_{\partial K}^2\right)^{1/2} \lesssim \left(\sum_{K\in\mathcal{T}_{f,h}} \sigma_f^{-1}\frac{l^2}{h_K}\left\|\widetilde{\boldsymbol{T}}_f(\boldsymbol{u}_h)\right\|_K^2\right)^{1/2}. \tag{13}$$

Since $\widetilde{\boldsymbol{T}}_f(\boldsymbol{u}) = \mathcal{C}_f \boldsymbol{D}(\boldsymbol{u})$, we have also

$$\left\|\widetilde{\boldsymbol{T}}_f(\boldsymbol{u}_h)\right\|_K \leq \bar{\mathcal{C}}_f^{1/2}\left(\widetilde{\boldsymbol{T}}_f(\boldsymbol{u}_h), \boldsymbol{D}(\boldsymbol{u}_h)\right)_K^{1/2}. \tag{14}$$

Now, putting together (11),(12),(13), and remembering the definition of σ_f in (7) and of the DG norm in (8), we obtain

$$
\begin{aligned}
A_{f,h}\left(\boldsymbol{u}_h,\boldsymbol{u}_h\right) \gtrsim\ & \frac{1}{2}\frac{d}{dt}\left\|\rho_f^{1/2}\boldsymbol{u}_h\right\|_{\Omega_f}^2 + \|\boldsymbol{u}_h\|_{DG,f}^2 \\
& - 2\left(\sum_{k\in\mathcal{T}_{f,h}} \sigma_f^{-1}\frac{l^2}{h_K}\bar{\mathcal{C}}_f\left(\widetilde{\boldsymbol{T}}_f(\boldsymbol{u}_h),\boldsymbol{D}(\boldsymbol{u}_h)\right)_K\right)^{1/2}\left\|\sigma_f^{1/2}[\![\boldsymbol{u}_h]\!]\right\|_{\mathcal{F}_{f,h}} \\
\geq\ & \frac{1}{2}\frac{d}{dt}\left\|\rho_f^{1/2}\boldsymbol{u}_h\right\|_{\Omega_f}^2 + \|\boldsymbol{u}_h\|_{DG,f}^2 \\
& - 2\gamma_f^{-1/2}\left(\sum_{k\in\mathcal{T}_{f,h}} \frac{h_K}{l^2\bar{\mathcal{C}}_f}\frac{l^2}{h_K}\bar{\mathcal{C}}_f\left(\widetilde{\boldsymbol{T}}_f(\boldsymbol{u}_h),\boldsymbol{D}(\boldsymbol{u}_h)\right)_K\right)^{1/2}\left\|\sigma_f^{1/2}[\![\boldsymbol{u}_h]\!]\right\|_{\mathcal{F}_{f,h}} \\
=\ & \frac{1}{2}\frac{d}{dt}\left\|\rho_f^{1/2}\boldsymbol{u}_h\right\|_{\Omega_f}^2 + \|\boldsymbol{u}_h\|_{DG,f}^2 - 2\gamma_f^{-1/2}a_f^{1/2}(\boldsymbol{u}_h,\boldsymbol{u}_h)\left\|\sigma_f^{1/2}[\![\boldsymbol{u}_h]\!]\right\|_{\mathcal{F}_{f,h}} \\
\geq\ & \frac{1}{2}\frac{d}{dt}\left\|\rho_f^{1/2}\boldsymbol{u}_h\right\|_{\Omega_f}^2 + \|\boldsymbol{u}_h\|_{DG,f}^2 - \gamma_f^{-1/2}a_f(\boldsymbol{u}_h,\boldsymbol{u}_h) - \gamma_f^{-1/2}\left\|\sigma_f^{1/2}[\![\boldsymbol{u}_h]\!]\right\|_{\mathcal{F}_{f,h}}^2,
\end{aligned}
$$

where in the last step we have used the Young's inequality. Now, taking γ_f large enough, we have that (10) holds true with $\alpha_f = 1-\gamma_f^{-1/2} \geq \overline{\alpha_f} > 0$, where $\overline{\alpha_f}$ is a positive constant bounded away from zero. □

Lemma 2. *The following equality holds true:*

$$
A_{s,h}\left(\widehat{\boldsymbol{d}}_h,\partial_t\widehat{\boldsymbol{d}}_h\right) = \frac{1}{2}\frac{d}{dt}\left(\left\|\widehat{\boldsymbol{d}}_h\right\|_{s,h}^2 - 2\left(\left\{\widehat{\boldsymbol{T}}_s(\widehat{\boldsymbol{d}}_h)\right\},[\![\widehat{\boldsymbol{d}}_h]\!]\right)_{\widehat{\mathcal{F}}_{s,h}}\right). \tag{15}
$$

Proof. The thesis easily follows by taking $\boldsymbol{w} = \partial_t\boldsymbol{d}$ in the definition of $A_{s,h}(\cdot,\cdot)$ in (6b), by remembering the definition of the norms in (8), and by noticing that by linearity

$$
\left(\left\{\widehat{\boldsymbol{T}}_s(\widehat{\boldsymbol{d}}_h)\right\},[\![\partial_t\widehat{\boldsymbol{d}}_h]\!]\right)_{\widehat{\mathcal{F}}_{s,h}} + \left([\![\widehat{\boldsymbol{d}}_h]\!],\left\{\widehat{\boldsymbol{T}}_s(\partial_t\widehat{\boldsymbol{d}}_h)\right\}\right)_{\widehat{\mathcal{F}}_{s,h}} = \frac{d}{dt}\left(\left(\left\{\widehat{\boldsymbol{T}}_s(\widehat{\boldsymbol{d}}_h)\right\},[\![\widehat{\boldsymbol{d}}_h]\!]\right)_{\widehat{\mathcal{F}}_{s,h}}\right).
$$

□

Lemma 3. *If Assumption 1 holds true for any element $K \in \mathcal{T}_{s,h}$, then the following inequalities hold true for any function $\widehat{\boldsymbol{w}}_h \in xxV_{s,h}^l$:*

$$
\begin{aligned}
\|\widehat{\boldsymbol{w}}_h\|_{s,h}^2 - 2\left(\left\{\widehat{\boldsymbol{T}}_s(\widehat{\boldsymbol{w}}_h)\right\},[\![\widehat{\boldsymbol{w}}_h]\!]\right)_{\widehat{\mathcal{F}}_{s,h}} &\gtrsim \|\widehat{\boldsymbol{w}}_h\|_{s,h}^2, \\
\|\widehat{\boldsymbol{w}}_h\|_{s,h}^2 - 2\left(\left\{\widehat{\boldsymbol{T}}_s(\widehat{\boldsymbol{w}}_h)\right\},[\![\widehat{\boldsymbol{w}}_h]\!]\right)_{\widehat{\mathcal{F}}_{s,h}} &\lesssim \|\widehat{\boldsymbol{w}}_h\|_{s,h}^2,
\end{aligned} \tag{16}
$$

where the first bound is valid provided that γ_s is large enough.

Proof. For the proof we refer the reader to [10, 12, 13]. $\square$

Lemma 4. *Set $\delta = 1$. Then, if γ_Σ is large enough and Assumption 1 holds true for any element $K \in \mathcal{T}_{f,h}$, there exists a positive constant α_Σ such that:*

$$A_{\Sigma,h}(\boldsymbol{u}_h, \boldsymbol{d}_h; \boldsymbol{u}_h, \partial_t \boldsymbol{d}_h) \gtrsim \alpha_\Sigma \left\| (\boldsymbol{u}_h, \boldsymbol{d}_h) \right\|_{\Sigma,h}^2 - \gamma_\Sigma^{-1/2} a_f(\boldsymbol{u}_h, \boldsymbol{u}_h). \tag{17}$$

Proof. From the definition of $A_{\Sigma,h}$ in (6c) and taking $\boldsymbol{v}_h = \boldsymbol{u}_h$ and $\boldsymbol{w}_h = \partial_t \boldsymbol{d}_h$, we obtain

$$A_{\Sigma,h}(\boldsymbol{u}_h, \boldsymbol{d}_h; \boldsymbol{u}_h, \partial_t \boldsymbol{d}_h) = -\left(\delta \widetilde{\boldsymbol{T}}_f(\boldsymbol{u}_h)\boldsymbol{n} + (1-\delta)\boldsymbol{T}_s(\boldsymbol{d}_h)\boldsymbol{n}, \boldsymbol{u}_h - \partial_t \boldsymbol{d}_h\right)_{\mathcal{F}_{\Sigma,h}}$$

$$-\left(\boldsymbol{u}_h - \partial_t \boldsymbol{d}_h, \delta \widetilde{\boldsymbol{T}}_f(\boldsymbol{u}_h)\boldsymbol{n} + (1-\delta)\boldsymbol{T}_s(\partial_t \boldsymbol{d}_h)\boldsymbol{n}\right)_{\mathcal{F}_{\Sigma,h}} + (\sigma_\Sigma(\boldsymbol{u}_h - \partial_t \boldsymbol{d}_h), \boldsymbol{u}_h - \partial_t \boldsymbol{d}_h)_{\mathcal{F}_{\Sigma,h}}.$$

Now, from the definition of the norms in (8) and by taking $\delta = 1$, we obtain

$$A_{\Sigma,h}(\boldsymbol{u}_h, \boldsymbol{d}_h; \boldsymbol{u}_h, \partial_t \boldsymbol{d}_h) = \left\| (\boldsymbol{u}_h, \boldsymbol{d}_h) \right\|_{\Sigma,h}^2 - 2\left(\widetilde{\boldsymbol{T}}_f(\boldsymbol{u}_h)\boldsymbol{n}, \boldsymbol{u}_h - \partial_t \boldsymbol{d}_h\right)_{\mathcal{F}_{\Sigma,h}}.$$

We notice that we have a result analogous to (12), since again the faces belonging to $\mathcal{F}_{\Sigma,h}$ are a subset of all the faces in $\mathcal{T}_{f,h}$:

$$\left\| \sigma_\Sigma^{-1/2} \widetilde{\boldsymbol{T}}_f(\boldsymbol{u}_h) \right\|_{\mathcal{F}_{\Sigma,h}} \lesssim \left(\sum_{k \in \mathcal{T}_{f,h}} \left\| \sigma_\Sigma^{-1/2} \widetilde{\boldsymbol{T}}_f(\boldsymbol{u}_h) \right\|_{\partial K}^2 \right)^{1/2} \lesssim \left(\sum_{k \in \mathcal{T}_{f,h}} \sigma_\Sigma^{-1} \frac{l^2}{h_K} \left\| \widetilde{\boldsymbol{T}}_f(\boldsymbol{u}_h) \right\|_K^2 \right)^{1/2}.$$

Now, proceeding in a similar way to Lemma 1, we obtain the thesis with $\alpha_\Sigma = \left(1 - \gamma_\Sigma^{-1/2}\right) \geq \overline{\alpha_\Sigma} > 0$, where $\overline{\alpha_\Sigma}$ is a positive constant bounded away from zero. $\square$

Finally, we can prove the main result of this section.

Theorem 1. *Set in (5) $\delta = 1$, and define*

$$\alpha_{f,\Sigma} = \alpha_f - \gamma_\Sigma^{-1/2} \geq \overline{\alpha_{f,\Sigma}} > 0, \tag{18}$$

where $\overline{\alpha_{f,\Sigma}}$ is a positive constant bounded away from zero. Then, if γ_f, γ_s, γ_Σ are large enough, Assumption 1 holds true for any element $K \in \mathcal{T}_{f,h} \bigcup \mathcal{T}_{s,h}$, $\boldsymbol{f}_f = \boldsymbol{0}$, and $\boldsymbol{f}_s = \boldsymbol{0}$, we have that the following stability bound holds true:

$$\left\| \rho_f^{1/2} \boldsymbol{u}_h(t) \right\|_{\Omega_f}^2 + 2\alpha_{f,\Sigma} \int_0^t \left\| \boldsymbol{u}_h(s) \right\|_{DG,f}^2 ds + \left\| \widehat{\boldsymbol{d}}_h(t) \right\|_{s,h}^2$$

$$+ 2\alpha_\Sigma \int_0^t \left\| (\boldsymbol{u}_h(s), \boldsymbol{d}_h(s)) \right\|_{\Sigma,h}^2 ds \lesssim \left\| \rho_f^{1/2} \boldsymbol{u}_h(0) \right\|_{\Omega_f}^2 + \left\| \widehat{\boldsymbol{d}}_h(0) \right\|_{s,h}^2,$$

where α_Σ is the constant of Lemma 4.

Proof. We start by noticing that taking $\boldsymbol{v}_h = \boldsymbol{u}_h$, $\widehat{\boldsymbol{w}}_h = \partial_t \widehat{\boldsymbol{d}}_h$ and $\boldsymbol{f}_f = \boldsymbol{f}_s = \mathbf{0}$ in (5), we obtain

$$A_{f,h}(\boldsymbol{u}_h, \boldsymbol{u}_h) + A_{s,h}\left(\widehat{\boldsymbol{d}}_h, \partial_t \widehat{\boldsymbol{d}}_h\right) + A_{\Sigma,h}(\boldsymbol{u}_h, \boldsymbol{d}_h; \boldsymbol{u}_h, \partial_t \boldsymbol{d}_h) = 0.$$

Now, using (10),(14),(16), and setting $\delta = 1$, we obtain

$$\frac{1}{2}\frac{d}{dt}\left\|\rho_f^{1/2}\boldsymbol{u}_h\right\|_{\Omega_f}^2 + \alpha_f \left\|\boldsymbol{u}_h\right\|_{DG,f}^2 + \frac{1}{2}\frac{d}{dt}\left(\left\|\widehat{\boldsymbol{d}}_h\right\|_{s,h}^2 - 2\left(\left\{\widehat{\boldsymbol{T}}_s(\widehat{\boldsymbol{d}}_h)\right\}, [\![\widehat{\boldsymbol{d}}_h]\!]\right)_{\widehat{\mathcal{F}}_{s,h}}\right)$$
$$+\alpha_\Sigma \left\|(\boldsymbol{u}_h, \boldsymbol{d}_h)\right\|_{\Sigma,h}^2 - \gamma_\Sigma^{-1/2} a_f(\boldsymbol{u}_h, \boldsymbol{u}_h) \lesssim 0.$$

Now, if γ_Σ is large enough, we have from (17) that $\alpha_{f,\Sigma} \geq \overline{\alpha_{f,\Sigma}} > 0$ for suitable positive constant $\overline{\alpha_{f,\Sigma}}$ bounded away from zero, and from the previous inequality we obtain

$$\frac{1}{2}\frac{d}{dt}\left\|\rho_f^{1/2}\boldsymbol{u}_h\right\|_{\Omega_f}^2 + \alpha_{f,\Sigma} \left\|\boldsymbol{u}_h\right\|_{DG,f}^2 + \frac{1}{2}\frac{d}{dt}\left(\left\|\widehat{\boldsymbol{d}}_h\right\|_{s,h}^2 - 2\left(\left\{\widehat{\boldsymbol{T}}_s(\widehat{\boldsymbol{d}}_h)\right\}, [\![\widehat{\boldsymbol{d}}_h]\!]\right)_{\widehat{\mathcal{F}}_{s,h}}\right) + \alpha_\Sigma \left\|(\boldsymbol{u}_h, \boldsymbol{d}_h)\right\|_{\Sigma,h}^2 \lesssim 0.$$

Integrating in time between 0 and t, we obtain

$$\left\|\rho_f^{1/2}\boldsymbol{u}_h(t)\right\|_{\Omega_f}^2 + 2\alpha_{f,\Sigma}\int_0^t \left\|\boldsymbol{u}_h(s)\right\|_{DG,f}^2 ds + \left\|\widehat{\boldsymbol{d}}_h(t)\right\|_{s,h}^2 - 2\left(\left\{\widehat{\boldsymbol{T}}_s(\widehat{\boldsymbol{d}}_h(t))\right\}, [\![\widehat{\boldsymbol{d}}_h(t)]\!]\right)_{\widehat{\mathcal{F}}_{s,h}}$$
$$+2\alpha_\Sigma \int_0^t \left\|(\boldsymbol{u}_h(s), \boldsymbol{d}_h(s))\right\|_{\Sigma,h}^2 ds \lesssim \left\|\rho_f^{1/2}\boldsymbol{u}_h(0)\right\|_{\Omega_f}^2 + \left\|\widehat{\boldsymbol{d}}_h(0)\right\|_{s,h}^2 - 2\left(\left\{\widehat{\boldsymbol{T}}_s(\widehat{\boldsymbol{d}}_h(0))\right\}, [\![\widehat{\boldsymbol{d}}_h(0)]\!]\right)_{\widehat{\mathcal{F}}_{s,h}}.$$

By using the inequalities (15), the thesis follows. □

3.3 Time discretization and treatment of the geometric coupling

For the time discretization, we consider a Backward Difference Formula of order p (BDFp) for the fluid and for the structure sub-problems. One major issue arising after time discretization is the treatment of the fluid domain. Indeed, due to the Eulerian framework, the fluid problem at time $t^n = n\Delta t$, $n = 0, 1, 2, \ldots$, Δt being the time discretization parameter, should be solved in the domain $\Omega_f^n \simeq \Omega_f(t^n)$. This introduces a source of non-linearity that needs to be properly managed. Classical choices are the implicit treatment obtained by means of sub-iterations (see, e.g., [57, 59, 68, 81]) and an inexact treatment based on a small fixed number of sub-iterations [77, 78]. Here, we considered instead an explicit treatment based on extrapolating the fluid domain position from the previous time steps [20,56]. In particular, according to the time discretization scheme, we consider $\Omega_f^n \simeq \Omega_f^*$, where Ω_f^* is a suitable p-th order extrapolation of previous domain Ω_f^m, $m = n-1, n-2, \ldots$, and $\Omega_f^m = \Omega \setminus \Omega_s^m = \Omega \setminus \left(\mathcal{L}_h^m\left(\widehat{\Omega}_s\right)\right)$, with $\mathcal{L}_h^m = I_{\widehat{\Omega}_s} + \widehat{\mathbf{d}}_h^m$ the discrete Lagrangian map. Thus, at time step t^n the FSI problem is solved by considering Ω_f^* as an approximation of Ω_f^n.

We notice that the fluid velocity at previous time steps appearing in the terms resulting from time discretization are not defined on Ω_f^* and then do not belong to the same space of the test functions $\boldsymbol{v}_h$ (remember that $\boldsymbol{V}_{f,h}^l$ changes in time, according to the mesh movement). Thus, these terms should be properly defined in the new computational domain Ω_f^* in order to be employed in the discrete formulation. Here we follow the idea proposed in [89]. In particular, whenever a fluid element at the previous time step t^{n-1} was partially covered by the structure, we obtain the solution at time t^n by extending it to the whole element itself by means of an extrapolation of order l (the space discretization order). In the case where the element was completely covered by the structure at time t^{n-1}, we extend in this element the numerical solution of a selected neighbour. For further details see [89].

4 Numerical results

In this section we present some numerical results to assess the practical performance of the proposed formulation, which has been implemented in *Matlab*. In particular, the DG spaces (3.1) are built in practice by using a modal expansion and based on employing a "bounding box" technique as described in [44], see also [11].

We consider the computational domain depicted in Figure 4, representing a thick structure immersed in a fluid. The fluid domain is a rectangle of size equal to $0.7\,cm \times 0.5\,cm$, whereas the size of the structure domain is $0.5\,cm \times 0.03\,cm$, whose bottom/left corner is placed in $(0.1, 0.235)\,cm$.

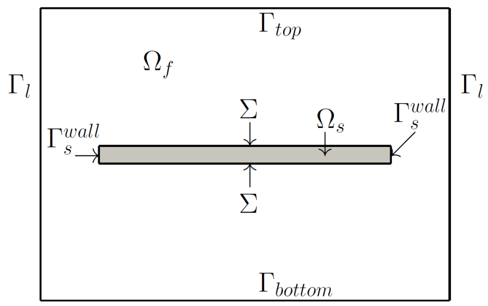

Figure 4: Fluid domain Ω_f and solid domain Ω_s (in grey) at the reference configuration used in the numerical experiments.

For the fluid sub-problem, we prescribe homogeneous Neumann conditions on Γ_{top} and Γ_{bottom} and homogeneous Dirichlet conditions on Γ_l, and set $\boldsymbol{f}_f = \boldsymbol{0}$. For the structure problem, we prescribe homogeneous Dirichlet conditions on

Γ_s^{wall} (fixed boundaries) and we set

$$\boldsymbol{f}_s\,(t) = \begin{cases} 100\,\widehat{\mathbf{j}}\,g/(cm^2s^2) & \text{if } t \in (0, 0.2)\,s, \\ \mathbf{0}\,g/(cm^2s^2) & \text{if } t \in [0.2, T]\,s, \end{cases}$$

where $\widehat{\mathbf{j}} = (0,1)$ and $T = 0.5\,s$. The other two portions of the structure boundaries coincide with the fluid-structure interface Σ. Thus, we expect to have an oscillation of the immersed structure along the y direction driven by the interaction with the surrounding fluid.

We use the following physical parameters: $\rho_f = 1\,g/cm^3$, $\lambda_f = 10^3\,g/(cm\,s)$, $\mu_f = 0.035\,g/(cm\,s)$, $\rho_s = 0.1\,g/cm^3$, $\lambda_s = 310\,Pa$, $\mu_s = 34\,Pa$. Moreover, we set $h \simeq 0.0125\,cm$ corresponding to about $5.8{\cdot}10^3$ elements for the fluid mesh, while we set $h \simeq 0.0083\,cm$ corresponding to about 500 elements for the structure mesh. In Figure 5, we report a zoom of the meshes close to the fluid-structure interface. We notice the non-conformity of the two meshes and the arbitrary shapes of the fluid mesh elements. Notice also the very small dimension of some fluid faces compared to the diameter of the corresponding element, that however does not compromise the stability of the numerical solutions. The time discretization parameter is

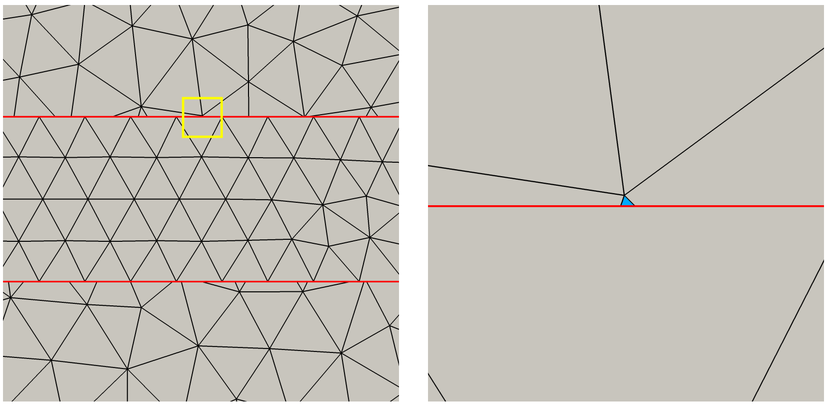

Figure 5: Left: zoom on the fluid and structure mesh (delimited by the red line). Right: further zoom inside the yellow box. A small fluid element (blue) appears near the immersed structure.

$\Delta t = 0.001\,s$. As for the penalty parameters in (7), we set $\gamma_\Sigma = \gamma_f = \gamma_s = 10$. In (5)-(6c), we set $\delta = 1$, that is, in accordance with the stability result in Theorem 1, we unbalance the average operator at the interface towards the fluid problem, see also [38]. We also set $p = l = 3$, where l is the polynomial approximation degree and p is the time discretization order. Thus, referring to Sect. 3.3, we have used the following extrapolation for the fluid domain Ω_f^n:

$$\Omega_f^* = 3\Omega_f^{n-1} - 3\Omega_f^{n-2} + \Omega_f^{n-3}.$$

The linear system arising at each time step after time discretization of (5) and corresponding to the proposed PolyDG discretization has been solved monolithically, thus avoiding the well-known *added mass* effect which heavily influences the convergence of partitioned schemes when the fluid density is comparable with (or even greater than) the structure one [19, 48, 58], as happens in our numerical experiments.

In Figure 6, we report the fluid velocity field and the displacement of the structure at five different time instants. From these results we observe the ability of our scheme to reproduce the structure dynamics.

In Figure 7 we report for three different time steps the evolution of the fluid mesh for $p = 3$. We observe in yellow a triangle which is initially uncovered, then cut by the structure mesh, and finally uncovered again due to the large structure displacement. To emphasize this scenario, we have used a coarser fluid mesh. To numerically manage this, we have implemented the strategy proposed in [89] and briefly described in Sect. 3.3.

Acknowledgement

The authors are members of the INdAM Research group GNCS and this work is partially funded by INDAM-GNCS. P.F. Antonietti has been also funded by SIR (Scientific Independence of young Researchers) starting grant n. RBSI14VT0S funded by MIUR - Italian Ministry of Education, University and Research. C. Vergara has been also supported by the H2020-MSCA-ITN-2017, EU project 765374 "ROMSOC - Reduced Order Modelling, Simulation and Optimization of Coupled systems".

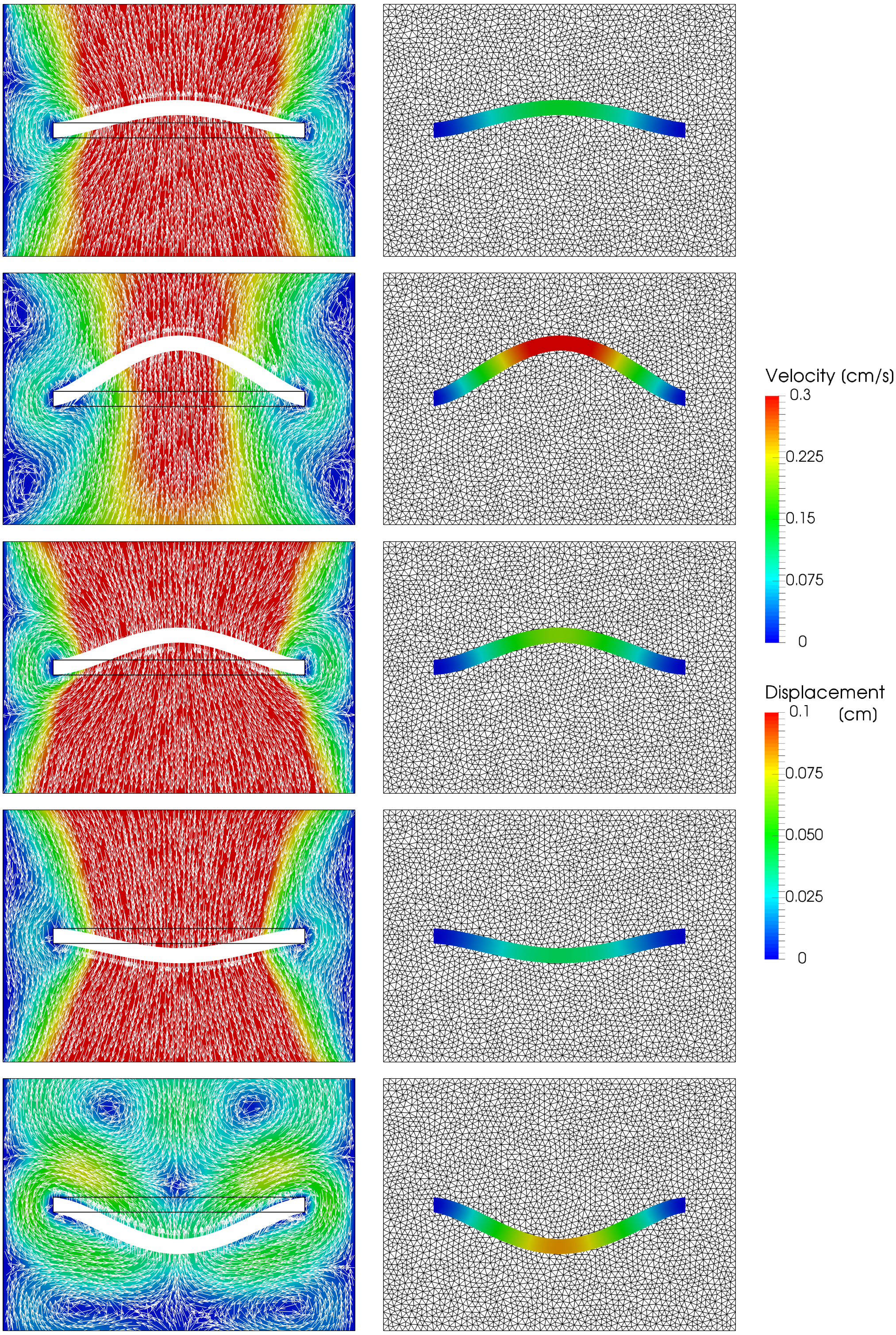

Figure 6: Fluid velocity (in cm/s) (left) and structure displacement (in cm) (right) at different observation times. From top to bottom: $t = 0.1\,s$, $t = 0.2\,s$, $t = 0.3\,s$, $t = 0.4\,s$ and $t = 0.5\,s$. $l = p = 3$.

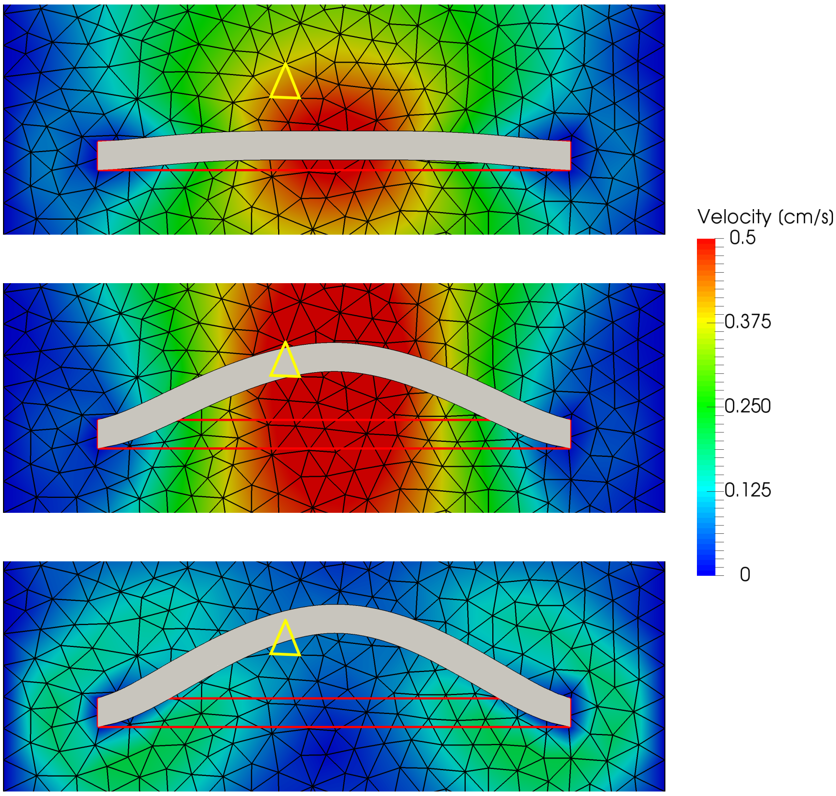

Figure 7: Fluid mesh evolution at different observation times. Top: $t = 0.05\,s$; middle: $t = 0.15\,s$; bottom: $t = 0.21\,s$. Colours represent the fluid velocity magnitude. $l = p = 3$.

References

[1] F. Alauzet, B. Fabrèges, M. A. Fernández, and M. Landajuela. Nitsche-XFEM for the coupling of an incompressible fluid with immersed thin-walled structures. *Comput. Methods Appl. Mech. Eng.*, 301:300–335, 2016.

[2] P. F. Antonietti, F. Brezzi, and L. D. Marini. Bubble stabilization of discontinuous galerkin methods. *Comput. Methods Appl. Mech. Engrg.*, 21-26(198):1651 – 1659, 2009.

[3] P. F. Antonietti, L. Beirão da Veiga, S. Scacchi, and M. Verani. A C1 Virtual Element Method for the Cahn-Hilliard equation with polygonal meshes. *SIAM J. Numer. Anal.*, 54(1):34 – 56, 2016.

[4] P. F. Antonietti, L. Formaggia, A. Scotti, M. Verani, and N. Verzotti. Mimetic Finite Difference approximation of flows in fractured porous media. *ESAIM Math. Model. Numer. Anal.*, 50(3):809 – 832, 2016.

[5] P. F. Antonietti, S. Giani, and P. Houston. *hp*-version Composite Discontinuous Galerkin methods for elliptic problems on complicated domains. *SIAM J. Sci. Comput.*, 35(3):A1417 – A1439, 2013.

[6] P. F. Antonietti, S. Giani, and P. Houston. *hp*-version composite Discontinuous Galerkin methods for elliptic problems on complicated domains. *SIAM J. Sci. Comput.*, 35(3):A1417 – A1439, 2013.

[7] P. F. Antonietti, S. Giani, and P. Houston. Domain decomposition preconditioners for discontinuous Galerkin methods for elliptic problems on complicated domains. *J. Sci. Comput.*, 60(1):203–227, 2014.

[8] P. F. Antonietti, P. Houston, X. Hu, M. Sarti, and M. Verani. Multigrid algorithms for *hp*-version Interior Penalty Discontinuous Galerkin methods on polygonal and polyhedral meshes. *Calcolo*, pages 1 – 30, 2017.

[9] Paola F. Antonietti, Gianmarco Manzini, and Marco Verani. The fully nonconforming Virtual Element method for biharmonic problems. *M3AS Math. Models Methods Appl. Sci.*, 28(2):387–407, 2018.

[10] P.F. Antonietti, F. Bonaldi, and I. Mazzieri. A high-order discontinuous Galerkin approach to the elasto-acoustic problem. *MOX Report 18/2018. Submitted.*

[11] P.F. Antonietti, A. Cangiani, J. Collis, Z. Dong, E.H. Georgoulis, S. Giani, and P. Houston. *Review of Discontinuous Galerkin Finite Element Methods for Partial Differential Equations on Complicated Domains*, pages 281–310. Springer, 1984.

[12] P.F. Antonietti, B. Ayuso de Dios, I. Mazzieri, and A. Quarteroni. Discontinuous Galerkin methods for the elastodynamics problem on polygonal and polyhedral meshes. *J. Sc. Comput.*, 68(1):143–170, 2016.

[13] P.F. Antonietti and I. Mazzieri. High-order Discontinuous Galerkin methods for the elastodynamics problem on polygonal and polyhedral meshes. *MOX Report 06/2018. Submitted.*

[14] P.F. Antonietti and G. Pennesi. V-cycle multigrid algorithms for discontinuous galerkin methods on non-nested polytopic meshes. *MOX Report 49/2017. Submitted.*

[15] P.F Antonietti, G. Pennesi, and P. Houston. Fast numerical integration on polytopic meshes with applications to discontinuous Galerkin finite element methods. *MOX Report 03/2018. Submitted.*

[16] D. N. Arnold, F. Brezzi, R.S. Falk, and L. D. Marini. Locking-free reissner-mindlin elements without reduced integration. *Comput. Methods Appl. Mech. Engrg.*, 196(37-40):3660–3671, 2007.

[17] D.N. Arnold, F. Brezzi, B. Cockburn, and L.D. Marini. Unified analysis of discontinuous galerkin methods for elliptic problems. *SIAM J. Numer. Anal.*, 39(5):1749–1779, 2001/2002.

[18] B. Ayuso de Dios, K. Lipnikov, and G. Manzini. The nonconforming Virtual Element Method. *ESAIM Math. Model. Numer. Anal.*, 50(3):879 – 904, 2016.

[19] S. Badia, F. Nobile, and C. Vergara. Fluid-structure partitioned procedures based on Robin transmission conditions. *J. Comput. Physics*, 227:7027–7051, 2008.

[20] S. Badia, A. Quaini, and A. Quarteroni. Splitting methods based on algebraic factorization for fluid-structure interaction. *SIAM J Sc Comp*, 30(4):1778–1805, 2008.

[21] F. Bassi, L. Botti, and A. Colombo. Agglomeration-based physical frame dG discretizations: an attempt to be mesh free. *Math. Mod. Meth. Appl. Sci.*, 24(8):1495–1539, 2014.

[22] F. Bassi, L. Botti, A. Colombo, D. A. Di Pietro, and P. Tesini. On the flexibility of agglomeration based physical space discontinuous Galerkin discretizations. *J. Comput. Phys.*, 231(1):45–65, 2012.

[23] F. Bassi, L. Botti, A. Colombo, and S. Rebay. Agglomeration based Discontinuous Galerkin discretization of the Euler and Navier-Stokes equations. *Comput. & Fluids*, 61:77–85, 2012.

[24] L. Beirão da Veiga, F. Brezzi, A. Cangiani, G. Manzini, L. D. Marini, and A. Russo. Basic principles of Virtual Element Methods. *Math. Models Methods Appl. Sci.*, 23(1):199 – 214, 2013.

[25] L. Beirão da Veiga, F. Brezzi, L. D. Marini, and A. Russo. Mixed Virtual Element Methods for general second order elliptic problems on polygonal meshes. *ESAIM Math. Model. Numer. Anal.*, 50(3):727 – 747, 2016.

[26] L. Beirão da Veiga, F. Brezzi, L. D. Marini, and A. Russo. Virtual Element Method for general second-order elliptic problems on polygonal meshes. *Math. Models Methods Appl. Sci.*, 26(4):729 – 750, 2016.

[27] L. Beirão da Veiga, K. Lipnikov, and G. Manzini. *The Mimetic Finite Difference method for elliptic problems*, volume 11. Springer, Cham, 2014.

[28] F. Benedettini, G. Rega, and R. Alaggio. Non-linear oscillations of a four-degree-of-freedom model of a suspended cable under multiple internal resonance conditions. *J. Sound Vibr.*, 182(5):775–798, 1995.

[29] M.F. Benedetto, S. Berrone, A. Borio, S. Pieraccini, and S. Scialo'. A hybrid mortar virtual element method for discrete fracture network simulations. *J. Comput. Phys.*, 306(1):148–166, 2016.

[30] M.F. Benedetto, S. Berrone, S. Pieraccini, and S. Scialo'. The virtual element method for discrete fracture network simulations. *Comput. Methods Appl. Mech. Engrg.*, 280(1):135–156, 2014.

[31] D. Boffi and L. Gastaldi. A finite element approach for the immersed boundary method. *Computers & Structures*, 81(8-11):491–501, 2003. K.J Bathe 60th Anniversary Issue.

[32] D. Boffi, L. Gastaldi, L. Heltai, and C. Peskin. On the hyper-elastic formulation of the immersed boundary method. *Comput. Methods Appl. Mech. Eng.*, 197(25–28):2210–2231, 2008.

[33] A. L. Braun and A. M. Awruch. Finite element simulation of the wind action over bridge sectional models: Application to the Guamá river bridge (Pará State, Brazil). *Finite Elements in Analysis and Design*, 44(3):105–122, 2008.

[34] F. Brezzi, K. Lipnikov, and M. Shashkov. Convergence of the Mimetic Finite Difference method for diffusion problems on polyhedral meshes. *SIAM J. Numer. Anal.*, 43(5):1872 – 1896 (electronic), 2005.

[35] F. Brezzi, K. Lipnikov, and M. Shashkov. Convergence of Mimetic Finite Difference method for diffusion problems on polyhedral meshes with curved faces. *Math. Mod. Meth. Appl. Sci.*, 16(2):275 – 297, 2006.

[36] F. Brezzi, K. Lipnikov, and V. Simoncini. A family of Mimetic Finite Difference methods on polygonal and polyhedral meshes. *Math. Mod. Meth. Appl. S.*, 15(10):1533 – 1551, 2005.

[37] E. Burman. Ghost penalty. *Comptes Rendus Mathematique*, 348(21):1217–1220, 2010.

[38] E. Burman and M. A. Fernández. An unfitted nitsche method for incompressible fluid-structure interaction using overlapping meshes. *Comput. Methods Appl. Mech. Eng.*, 279:497–514, 2014.

[39] E. Burman and M.A. Fernández. Stabilized explicit coupling for fluid-structure interaction using Nitsche's method. *C. R. Acad. Sci. Paris Sér. I Math.*, 345:467–472, 2007.

[40] E. Burman and M.A. Fernández. Stabilization of explicit coupling in fluid-structure interaction involving fluid incompressibility. *Comp. Meth. Appl. Mech Eng.*, 198(5-8):766–784, 2009.

[41] A. Cangiani, Z. Dong, and E. H. Georgoulis. *hp*-Version space-time discontinuous Galerkin methods for parabolic problems on prismatic meshes. *SIAM J. Sci. Comput.*, 39(4):A1251 – A1279, 2017.

[42] A. Cangiani, Z. Dong, E. H. Georgoulis, and P. Houston. *hp*-Version discontinuous Galerkin methods for advection-diffusion-reaction problems on polytopic meshes. *ESAIM Math. Model. Numer. Anal.*, 50:699 – 725, 2016.

[43] A. Cangiani, Z. Dong, E. H. Georgoulis, and P. Houston. *hp-Version Discontinuous Galerkin Methods on Polygonal and Polyhedral Meshes*. Springer Briefs in Mathematics, Springer, 2017.

[44] A. Cangiani, E. H. Georgoulis, and P. Houston. *hp*-Version discontinuous Galerkin methods on polygonal and polyhedral meshes. *Math. Models Methods Appl. Sci.*, 24(10):2009 – 2041, 2014.

[45] A. Cangiani, E.H. Georgoulis, and Y. Sabawi. Adaptive discontinuous Galerkin methods for elliptic interface problems. *Math. Comp.*, (in press), 2017.

[46] A. Cangiani, G. Manzini, and O. J. Sutton. Conforming and nonconforming Virtual Element Methods for elliptic problems. *IMA J. Numer. Anal.*, 37(3):1317 – 1354, 2017.

[47] G.F Carey and R. Krishnan. Penalty approximation of Stokes flow. *Comput. Methods Appl. Mech. Engrg.*, 35:169–206, 1982.

[48] P. Causin, J.F. Gerbeau, and F. Nobile. Added-mass effect in the design of partitioned algorithms for fluid-structure problems. *Comput. Methods Appl. Mech. Engrg.*, 194(42-44):4506–4527, 2005.

[49] B. Cockburn, B. Dond, and J. Guzmán. A superconvergent LDG-hybridizable Galerkin method for second-order elliptic problems. *Math. Comp.*, 77(264):1887–1916, 2008.

[50] J. De Hart, F.P.T. Baaijens, G.W.M. Peters, and P.J.G. Schreurs. A computational fluid-structure interaction analysis of a fiber-reinforced stentless aortic valve. *J. Biomech.*, 36(5):699 – 712, 2003. Cardiovascular Biomechanics.

[51] D. A. Di Pietro and A. Ern. A Hybrid High-Order locking-free method for linear elasticity on general meshes. *Comput. Methods Appl. Mech. Engrg.*, 283(1):1 – 21, 2015.

[52] D. A. Di Pietro and A. Ern. Hybrid High-Order methods for variable-diffusion problems on general meshes. *C. R. Math. Acad. Sci. Soc. R. Can.*, 353(1):31 – 34, January 2015.

[53] D. A. Di Pietro, A. Ern, and S. Lemaire. An arbitrary-order and compact-stencil discretization of diffusion on general meshes based on local reconstruction operators. *Comput. Method Appl. Math.*, 14(4):461 – 472, October 2014.

[54] J. Donea. An arbitrary Lagrangian-Eulerian finite element method for transient dynamic fluid-structure interaction. *Comp. Methods Applied Mech. Engineering*, 33:689–723, 1982.

[55] J. Droniou, R. Eymard, and R. Herbin. Gradient schemes: generic tools for the numerical analysis of diffusion equations. *ESAIM Math. Model. Numer. Anal.*, 50(3):749 – 781, 2016.

[56] M.A. Fernández, J.F. Gerbeau, and C. Grandmont. A projection semi-implicit scheme for the coupling of an elastic structure with an incompressible fluid. *Int. J. Num. Methods Engrg.*, 69(4):794–821, 2007.

[57] M.A. Fernández and M. Moubachir. A Newton method using exact Jacobians for solving fluid-structure coupling. *Comput. Struct.*, 83(2-3):127–142, 2005.

[58] C. Forster, W. Wall, and E. Ramm. Artificial added mass instabilities in sequential staggered coupling of nonlinear structures and incompressible viscous flow. *Comput. Methods Appl. Mech. Engrg.*, 196(7):1278–1293, 2007.

[59] M.W. Gee, U. Kuttler, and W.A. Wall. Truly monolithic algebraic multigrid for fluid-structure interaction. *Int. J. Num. Methods Engrg.*, 85(8):987–1016, 2011.

[60] S. Giani and P. Houston. *hp*-Adaptive composite Discontinuous Galerkin methods for elliptic problems on complicated domains. *Numer. Methods Part. Diff. Eq.*, 30(4):1342 – 1367, 2014.

[61] R. Glowinski, T.-W. Pan, T. I. Hesla, and D. D. Joseph. A distributed lagrange multiplier/fictitious domain method for particulate flows. *Int. J. Multiph. Fl.*, 25(5):755–794, 1999.

[62] B.E. Griffith, X. Luo, D.M. McQueen, and C.S. Peskin. Simulating the fluid dynamics of natural and prosthetic heart valves using the immersed boundary method. *Int. J. Appl. Mech.*, 1:137–176, 2009.

[63] W. Hackbusch and S. A. Sauter. Composite Finite Elements for problems containing small geometric details. Part II: Implementation and numerical results. *Comput. Visual Sci.*, 1(4):15–25, 1997.

[64] W. Hackbusch and S. A. Sauter. Composite Finite Elements for the approximation of PDEs on domains with complicated micro-structures. *Numer. Math.*, 75(4):447–472, 1997.

[65] S. Haeri and J. S. Shrimpton. On the application of immersed boundary, fictitious domain and body-conformal mesh methods to many particle multiphase flows. *Int. J. Multiph. Fl.*, 40:38–55, April 2012.

[66] A. Hansbo and P. Hansbo. An unfitted finite element method, based on nitsches method, for elliptic interface problems. *Comput. Methods Appl. Mech. Eng.*, 191(47–48):5537–5552, 2002.

[67] Z. Harun, E. Reda, and S. Abdullah. Large eddy simulation of the wind flow over skyscrapers. *Recent Adv. Mech. Mech. Eng.*, 15:72–79, 2015.

[68] M. Heil. An efficient solver for the fully coupled solution of large-displacement fluid-structure interaction problems. *Comput. Methods Appl. Mech. Engrg.*, 193:1–23, 2004.

[69] T.J.R. Hughes, W.K. Liu, and A. Brooks. Finite element analysis of incompressible viscous flows by the penalty function formulation. *J. Comput. Physics*, 30:1–60, 1979.

[70] J. Hyman, M. Shashkov, and S. Steinberg. The numerical solution of diffusion problems in strongly heterogeneous non-isotropic materials. *J. Comput. Phys.*, 132(1):130 – 148, 1997.

[71] Y. G. Lai, K. B. Chandran, and J. Lemmon. A numerical simulation of mechanical heart valve closure fluid dynamics. *J. Biomech.*, 35(7):881–892, 2002.

[72] K. Lipnikov, D. Vassilev, and I. Yotov. Discontinuous Galerkin and mimetic finite difference methods for coupled Stokes-Darcy flows on polygonal and polyhedral grids. *Numer. Math.*, 126(2):321 – 360, 2014.

[73] G. Marom, H.-S. Kim, M. Rosenfeld, E. Raanani, and R. Haj-Ali. Fully coupled fluid-structure interaction model of congenital bicuspid aortic valves: effect of asymmetry on hemodynamics. *Med. Biol. Engineering and Computing*, 51(8):839–848, 2013.

[74] A. Massing, M. G. Larson, and A. Logg. Efficient implementation of finite element methods on nonmatching and overlapping meshes in three dimensions. *SIAM J. Sc. Comput.*, 35(1):C23–C47, 2013.

[75] R. Mittal and G. Iaccarino. Immersed boundary methods. *Annual Review of Fluid Mechanics*, 37(1):239–261, 2005.

[76] F. Müller, D. Schötzau, and C. Schwab. Symmetric interior penalty discontinuous Galerkin methods for elliptic problems in polygons. *SIAM J. Num. Anal.*, 55(5):2490–2521, 2017.

[77] F. Nobile, M. Pozzoli, and C. Vergara. Time accurate partitioned algorithms for the solution of fluid-structure interaction problems in haemodynamics. *Comp. Fl.*, 86:470–482, 2013.

[78] F. Nobile, M. Pozzoli, and C. Vergara. Inexact accurate partitioned algorithms for fluid-structure interaction problems with finite elasticity in haemodynamics. *J. Comput. Phys.*, 273:598–617, 2014.

[79] C. Peskin. Flow patterns around heart valves: A numerical method. *J. Comput Phys.*, 10(2):252–271, 1972.

[80] C. Peskin. The immersed boundary method. *Acta Numerica*, 11:479–517, 1 2002.

[81] A. Quarteroni, A. Manzoni, and C. Vergara. The cardiovascular system: Mathematical modelling, numerical algorithms and clinical applications. *Acta Numerica*, 26:365–590, 2017.

[82] G. Rega. Nonlinear vibrations of suspended cables–Part I: Modeling and analysis. *Appl. Mech. Rev.*, 57(6):443–478, 2004.

[83] F. Sturla, E. Votta, M. Stevanella, C. A. Conti, and A. Redaelli. Impact of modeling fluid-structure interaction in the computational analysis of aortic root biomechanics. *Med. Eng. Phys.*, 35(12):1721–1730, 2013.

[84] N. Sukumar and A. Tabarraei. Conforming Polygonal Finite Elements. *Internat. J. Numer. Methods Engrg.*, 61(12):2045–2066, 2004.

[85] R. Temam. *Navier Stokes equations - Theory and numerical analysis.* AMS Chelsea puplishing, 2000.

[86] E. J. Weinberg and M. R. Kaazempur Mofrad. Transient, three-dimensional, multiscale simulations of the human aortic valve. *Card. Eng.*, 7(4):140–155, 2007.

[87] D. Wiresaet, E. J. Kubatko, C. E. Michoski, S. Tanaka, J. J. Westerink, and C. Dawson. Discontinuous Galerkin methods with nodal and hybrid modal/nodal triangular, quadrilateral, and polygonal elements for nonlinear shallow water flow. *Comput. Methods Appl. Mech. Engrg.*, 270:113 – 149, 2014.

[88] H. Zhang, L. Liu, M. Dong, and H. Sun. Analysis of wind-induced vibration of fluid–structure interaction system for isolated aqueduct bridge. *Eng. Struct.*, 46:28–37, 2013.

[89] S. Zonca, C. Vergara, and L. Formaggia. An unfitted formulation for the interaction of an incompressible fluid with a thick structure via an XFEM/DG approach. *SIAM J. Sc. Comput.*, (40(1)):B59–B84, 2017.

MOX Technical Reports, last issues

Dipartimento di Matematica
Politecnico di Milano, Via Bonardi 9 - 20133 Milano (Italy)

25/2018 Chave, F.; Di Pietro, D.A.; Formaggia, L.
A Hybrid High-Order method for passive transport in fractured porous media

26/2018 Vergara, C.; Zonca, S.
Extended Finite Elements method for fluid-structure interaction with an immersed thick non-linear structure

24/2018 Bassi, C.; Abbà, A.; Bonaventura,L.; Valdettaro,L.
Direct and Large Eddy Simulation of three-dimensional non-Boussinesq gravity currents with a high order DG method

23/2018 Benacchio, T.;Bonaventura,L.
A seamless extension of DG methods for hyperbolic problems to unbounded domains

22/2018 Pegolotti, L.; Dede', L.; Quarteroni, A.
Isogeometric Analysis of the electrophysiology in the human heart: numerical simulation of the bidomain equations on the atria

21/2018 Gervasio, P.; Dede', L.; Chanon, O.; Quarteroni, A.
Comparing Isogeometric Analysis and Spectral Element Methods: accuracy and spectral properties

20/2018 Bassi, C. ; Abbà, A.; Bonaventura L.; Valdettaro, L.
A priori tests of a novel LES approach to compressible variable density turbulence

19/2018 Menghini, F.; Dede', L.; Quarteroni, A.
Variational Multiscale LES modeling of blood flow in an idealized left human heart

18/2018 Antonietti, P.F.; Bonaldi, F.; Mazzieri, I.
A high-order discontinuous Galerkin approach to the elasto-acoustic problem

17/2018 Agosti, A.; Giverso, C.; Faggiano, E.;Stamm,A.; Ciarletta, P.
A personalized mathematical tool for neuro-oncology: a clinical case study